

# A Centralized Ship Localization Strategy for Passive Multistatic Radar Based on Navigation Satellites

Ilaria Nasso, Fabrizio Santi

**Abstract**—This letter focuses on ship target localization using a multistatic passive radar system based on navigation satellites opportunistic illuminators. In such systems, the typical approach to localize the targets is taking peripheral decisions at each bistatic channel to detect the target followed by bistatic ranges intersection. In contrast, here we consider a centralized approach in order to jointly detect and localize the ship target of interest. The proposed approach entirely operates in a Cartesian plane representing the surveyed maritime area and it is able to combine the signals pertaining the different bistatic links despite the variation of the e.m. response of the targets, typically occurring in the framework under consideration as the target is illuminated by multiple (and possibly widely separated) transmitters viewing angles. Moreover, the hypothesis of point-like targets is here replaced with the more realistic case of extended targets (i.e., occupying more than one resolution cell). The ship localization effectiveness of the method is proved via both synthetic and experimental datasets.

**Index Terms**—passive multistatic radar, GNSS-based passive radar, maritime surveillance, ship localization.

## I. INTRODUCTION

PASSIVE radar systems based on Global Navigation Satellite Systems (GNSS) signals are a promising option for maritime surveillance applications. In addition to the well-known benefits of passive sensors such as cost effectiveness, absence of harmful radiations and covertness, the ubiquitous and persistent nature of navigation signals enable coverage in both coastal and open sea areas [1]. However, the major feature of GNSS stays in the constellation design, which guarantees the simultaneous illumination from multiple satellites allowing multistatic operations using a single receiving station [2]–[6].

In this type of configuration, ship detection and localization are usually obtained by resorting to decentralized strategies: peripheral decisions are taken at each bistatic link and subsequently the target position is estimated by intersecting the ellipsoids defined by the bistatic ranges [2][3]. However, the main shortcoming of GNSS-based passive radar system is the restricted power budget, requiring advanced signal processing techniques to increase the ships observability. E.g., techniques able to integrate up to 30s of data could be needed to detect a

target with Radar Cross Section (RCS) 30 dBm<sup>2</sup> at ~9 and 13 km range with a single [7] and four satellites [4], respectively. Moreover, ship localization requires it to be detected over a minimum number of links, with the further issue represented by the data association [8].

As well-known, centralized approaches can achieve superior performance than their decentralized counterparts [9]. Indeed, decentralized procedures perform data fusion at the level of plots (i.e., after thresholding), and therefore they do not manage to fully benefit of bistatic geometries providing stronger signal power, whereas missed detections in those bistatic channels providing a too low RCS can partially or completely compromise the possibility to localize the ship. In contrast, in centralized approaches, the data are combined in square amplitudes: by avoiding the hard decision taken at each channel, the information contained in the worse links (i.e., those that would give rise to a missed detection event) is not discarded, while the contribution of the channels showing the highest signal-to-noise ratio (SNR) is maximized [10].

In this letter, we propose a data processing strategy to combine the data in a centralized fashion. It is worth to point out that centralized data fusion strategies are particular appealing for the system under consideration, as the large spatial diversity characterizing GNSS illuminators can make the target RCS considerably vary among the bistatic channels. Moreover, the receiver acts as collector of the multichannel data, so that setting a broadband communication channel among the nodes of the multistatic configuration is not required. The proposed approach implements two types of integrations: (i) over the temporal domain, i.e., combining multiple frames corresponding to consecutive Coherent Processing Intervals (CPIs) and (ii) over the space domain, i.e., over the multiple bistatic geometries corresponding to different satellites. A similar approach operating in the Range-Doppler (RD) domain has been proposed in [4]. In contrast, the approach here considered operates entirely in the Cartesian domain, thus providing a clear picture of the surveyed area and allowing a direct localization of the ship.

The proposed technique is a modified version of the local-plane based technique originally proposed in [7] for bistatic configurations and here extended to the multistatic case. Moreover, unlike previous works, the point-like target assumption is here replaced with a more realistic model of extended target. Indeed, with the modernization of the GNSS signals, relatively wide bandwidths are nowadays available: e.g., Galileo E5a/b and GPS L5 emit pseudo random noise

Manuscript received XXXXX; revised YYYYY

The authors are with the Department of Information Engineering Electronics and Telecommunications, Sapienza University of Rome, 00184 Rome, Italy (email: ).

Color versions of one or more of the figures in this article are available online at <http://ieeexplore.ieee.org>  
Digital Object Identifier ZZZZ/LGRS.ZZZZZ

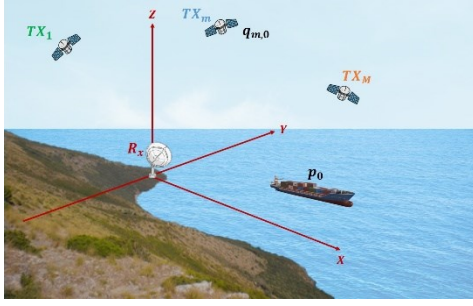


Fig. 1. System geometry.

(PRN) sequences with a bandwidth of 10.23 MHz. This results in range resolutions up to 15 m, therefore better than most of ship target extents. As ship targets are characterized by complex structures (including superstructures), shadowing effects likely appear so that different parts of the target could be visible under widely separated illumination angles [11]. Consequently, ranges pertaining different scattering centers may be intersected in decentralized procedures, potentially carrying to significant errors in localization. The focus of this work is showing as the proposed centralized strategy can enhance the localization performance with respect to decentralized approaches.

Section II details the proposed approach, while in Section III few simulated case studies are shown to analyze its potentialities in ship localization. Experimental results are provided in Section IV and Section V closes the letter.

## II SYSTEM OVERVIEW AND CENTRALIZED PROCESSING SCHEME

The operative conditions comprise a passive device located in a remote location above the sea and  $M$  GNSS satellites. The receiver registers their direct signals via a wide-beam antenna pointed toward the sky (reference channel) while the signal reflections are recorded via a surveillance channel using a high-gain antenna steered toward the surveyed area. Fig. 1 shows the right-handed  $(0, X, Y, Z)$  reference system, centered in the receiver position. The ground plane  $(X, Y)$  represents the maritime surveyed area where the  $X$ -axis is aligned with the surveillance channel antenna pointing direction.

In decentralized procedures, the target is detected in the RD maps pertaining the  $M$  satellites and the corresponding isoranges are intersected for the localization task. Due to the very low flux power density of the GNSS signals over the Earth 'surface, detection probability in the individual maps is poor and a few techniques have been recently proposed to extend the integration time thus reinforcing the received power [7][12][13]. Typically, a long-time map is achieved by multi-frame integration of consecutive RD maps subsequent to target motion compensation procedures. Nevertheless, in those channels experiencing a too low bistatic RCS, this might not suffice, giving rise to missed detections. To overcome this limitation and enhance system performance, the proposed centralized strategy performs an integration in both the time (multi-frame) and space (multi-transmitter) domains. The processing chain is depicted in Fig. 2 and it includes the following stages.

*Preprocessing* - As GNSS signals are CW, data are preliminary transformed into the equivalent of fast-time and slow time according to a fictitious pulse repetition time (PRT),

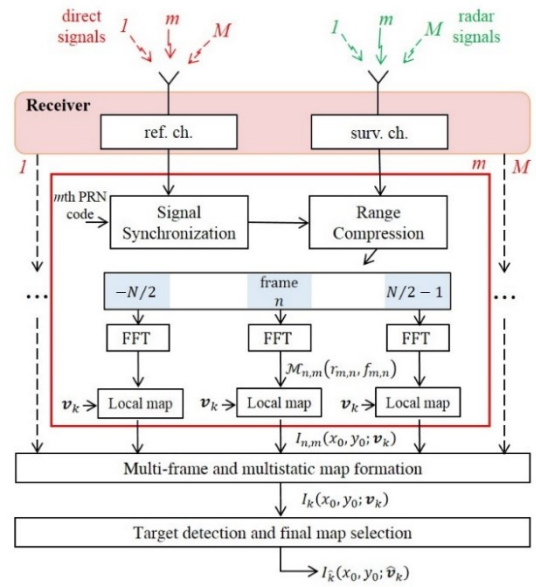


Fig. 2. Centralized processing scheme.

typically equal to 1 ms. Then, range compression is implemented by cross-correlating the surveillance channel data with the locally generated replica of the direct signal achieved via signal synchronization algorithms [1]. Noticeably, as the codes used by GNSS are quasi-orthogonal, the different satellites can be separately processed.

*RD maps formation* - The range compressed data are segmented in  $N$  consecutive frames, having each duration  $T_f$  (i.e., CPI). By means of Fast Fourier Transforms over the slow-time, a RD map is obtained for each frame and for each bistatic channel. By setting a limited CPI (2-3 sec [1]), target reflectivity can be assumed constant inside each frame. Moreover, taking into account the relatively low speed of ship targets, intra-frame range and Doppler migration can be neglected. Particularly, as shown in [7], target migration in each frame can be neglected for targets not very close to the receiver, i.e., for those targets mainly requiring multi-frame and multistatic integration to strengthen their received power.

Let  $\mathcal{M}_{n,m}$  be the RD map corresponding to the  $n$ th frame ( $n = -N/2, \dots, N/2 - 1$ ) and  $m$ th ( $m = 1, \dots, M$ ) baseline and let  $\mathbf{p}_n = \mathbf{p}_0 + \mathbf{v}u_n$  and  $\mathbf{q}_{m,n} = \mathbf{q}_{m,0} + \mathbf{v}_m u_n$  be the target and  $m$ th satellite Cartesian positions at the  $n$ th frame time, where  $\mathbf{p}_0$  and  $\mathbf{q}_{m,0}$  denote the positions at the reference frame instant  $n = 0$ ,  $\mathbf{v}$  and  $\mathbf{v}_m$  are the target and  $m$ th satellite velocity vectors, and  $u_n = nT_f$  is the frame time. In the  $(m, n)$ th RD map, target range and Doppler positions are equal to

$$r_{m,n} = \|\mathbf{q}_{m,0} - \mathbf{p}_0 + (\mathbf{v}_m - \mathbf{v})u_n\|_2 + \|\mathbf{p}_0 + \mathbf{v}u_n\|_2 - \|\mathbf{q}_{m,0} + \mathbf{v}_m u_n\|_2 \quad (1)$$

$$f_{m,n} = -\frac{1}{\lambda} \frac{\partial r_{m,n}}{\partial u_n} = -\frac{1}{\lambda} \left( \frac{(\mathbf{q}_{m,0} - \mathbf{p}_0)(\mathbf{v}_m - \mathbf{v}) + \|\mathbf{v}_m - \mathbf{v}\|_2^2}{\|\mathbf{q}_{m,0} - \mathbf{p}_0 + (\mathbf{v}_m - \mathbf{v})u_n\|_2} + \frac{\mathbf{p}_0^T \mathbf{v} + \|\mathbf{v}\|_2^2}{\|\mathbf{p}_0 + \mathbf{v}u_n\|_2} - \frac{\mathbf{q}_{m,0}^T \mathbf{v}_m + \|\mathbf{v}_m\|_2^2}{\|\mathbf{q}_{m,0} + \mathbf{v}_m u_n\|_2} \right) \quad (2)$$

where  $\lambda$  is the carrier wavelength and  $\|\cdot\|_2$  denotes the Euclidian norm. As the focus is on ship targets, we can assume  $\mathbf{p}_0 = [x_0, y_0, 0]^T$  and  $\mathbf{v} = [v_x, v_y, 0]^T$ .

*Local maps generation* – To perform an integration of the individual maps on a pixel basis, each RD map is projected into a local (i.e., Cartesian) map corresponding to the scene at the reference time instant (referred as to local map). To this purpose, for each hypothesized position  $(x_0, y_0)$  occupied by the target at the reference time instant, the corresponding range and Doppler position in each  $\mathcal{M}_{n,m}$  are calculated via (1) and (2) and the value in the selected cell is stored in a local map. As GNSS message contains the satellite instantaneous position  $\mathbf{q}_{m,n}$ , the receiver has a complete knowledge of the system topology and the selection of the  $(m, n)$ th RD cell depends on the target velocity only. As this is unknown, the procedure must be implemented for an admissible set of target velocity vectors. Therefore, for each tested target velocity  $\mathbf{v}_k$ , from each RD map  $\mathcal{M}_{n,m}$  a local map  $I_{n,m}(x_0, y_0; \mathbf{v}_k)$  is obtained.

*Multi-frame and multistatic map formation and selection* – For each tested velocity, the procedure above generates  $NM$  local maps in a common reference system independent on the particular frame/baseline. Therefore, an integrated map can be straightforwardly achieved via quadratic integration:

$$I_k(x_0, y_0; \mathbf{v}_k) = \sum_{m=1}^M \sum_{n=-N/2}^{N/2-1} |I_{n,m}(x_0, y_0; \mathbf{v}_k)|^2 \quad (3)$$

The capability of the technique to follow the RD history of the target over the different frames, namely to select the correct set of cells, depends on the tested velocity. In the  $I_{n,m}$  maps, scatterers ‘energy concentrate in the position occupied at the reference time if the procedure is driven by the actual velocity vector. Therefore, the maximum integration gain is achieved in the integrated map for  $\mathbf{v}_k$  closest to the actual velocity. In this map, the target can be therefore detected and directly localized on the Cartesian plane. However, depending on the particular conditions (i.e., SNR in input to the receiver), detections can occur also in maps corresponding to different tested velocities, where the scatterers energy concentrates around positions different from the correct ones.

Considering the possibility that the target does not behave like a point source but distributes over different resolution cells, the final map is selected according to a ‘global’ view of the energy spread: among the maps where the target has been detected, the final map is selected as the one corresponding to the velocity providing the maximum Intensity Contrast (IC), i.e.,

$$\hat{\mathbf{v}} = \max_{\mathbf{v}_k} \left\{ \sqrt{E[I_k - E[I_k]]^2 / E[I_k]} \right\} \quad (4)$$

$E[*]$  denoting the average value of the pixels corresponding to the target area.

We point out that in the case of multiple targets, the well-known ‘ghost’ phenomenon could occur [9]. However, the multi-frame and multistatic integration procedure acts like a space-time ghost rejection filter, as the greater is the number of frames/satellites, the less likely it is the possibility that the energy of different targets will be registered in the final map.

### III SHIP LOCALIZATION RESULTS

The higher detection performance of centralized than

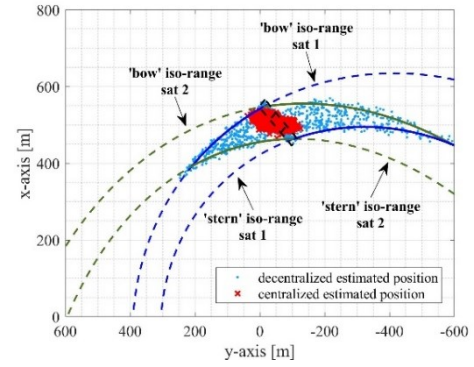


Fig. 3. Centralized vs decentralized position estimations.

decentralized procedures are well documented in literature. Therefore, this section is devoted at showing the greater capability of the proposed approach to localize a ship despite its extent over multiple resolution cells and the variation of its signature over multiple bistatic channels. A few case studies are considered assuming a ship with size  $144 \text{ m} \times 27 \text{ m}$  (i.e., compliant with the opportunistic target considered in the next section) sailing in the receiver field of view with its center of gravity in  $[506 \text{ m}, -57 \text{ m}]$  at the reference instant and moving with velocity  $[3, 3] \text{ m/s}$ . The target is supposed illuminated by two Galileo transmitters with aspect angles (measured clockwise from X-axis)  $102^\circ$  and  $159^\circ$  and elevation angles  $56^\circ$  and  $49^\circ$ . E5a band signals (carrier frequency  $1176.45 \text{ MHz}$  and chip-rate  $10.23 \text{ MHz}$ ) are used for the radar processing.

In a first case study, the target is assumed composed by three main scatterers located respectively in the ‘bow’, ‘central’, and ‘stern’ areas, each of  $48 \text{ m} \times 27 \text{ m}$  along the ship centerline. To simulate the variation of the target signature with the different bistatic geometries, scatterer positions are modeled as random variables uniformly distributed within the three areas and uncorrelated between the bistatic geometries. Moreover, in each channel, one scatterer is supposed to be dominant whereas the other two provide a lower return. Although this cannot be considered a precise model of a ship target signature, which can be a formidable task well beyond the scope of this letter, it is well in line with results experimentally achieved (see [5] and the experimental results provided in the next section). Monte Carlo simulations (1000 independent trials) are carried out randomly selecting in each trial and independently for the two baselines the scatterer providing the stronger return. For each trial and for each satellite,  $N = 10$  RD maps with  $T_f = 3 \text{ s}$  are generated by adding white Gaussian noise. The stronger and weaker scatterers provide SNR equal to  $10 \text{ dB}$  and  $1 \text{ dB}$  in the single frame maps. For the decentralized procedure, two multi-frame bistatic RD maps are produced by quadratic integration of the  $N$  maps subsequently an ideal compensation of the target frame-to-frame migration, while by means of the proposed centralized strategy using the actual target velocity, an integrated local map is obtained. In both the cases, the target is detected by applying a threshold according to a false alarm rate of  $10^{-3}$  (as the focus here is on localization performance, SNR suitable to achieve a detection probability  $\sim 100\%$  with both the decentralized and centralized strategies has been considered). The target RD/Cartesian position is evaluated as the central



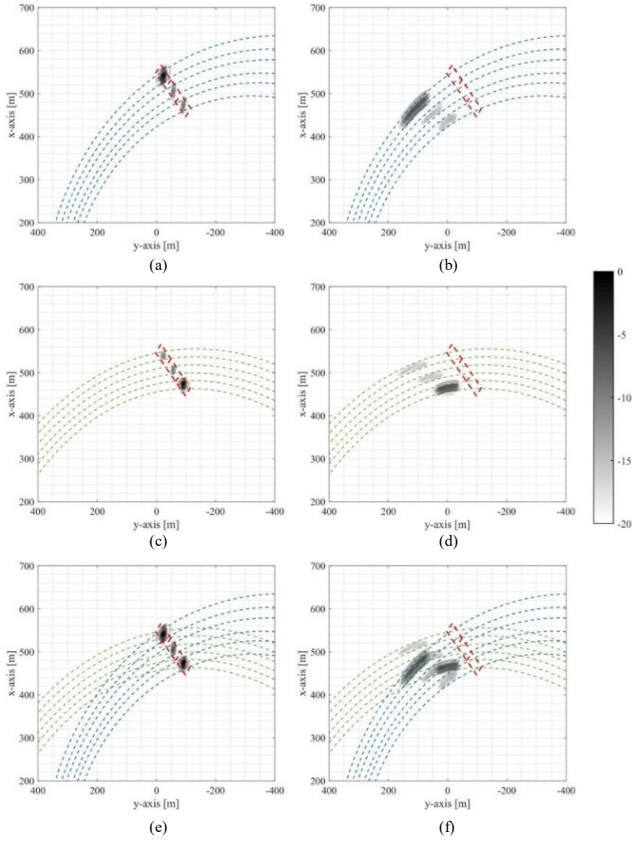


Fig. 4. Local maps for different tested velocities – (a) sat. 1,  $\mathbf{v}_1$ ; (b) sat. 1,  $\mathbf{v}_2$ ; (c) sat. 2,  $\mathbf{v}_1$ ; (d) sat. 2,  $\mathbf{v}_2$ ; (e) sat. 1 + sat. 2,  $\mathbf{v}_1$ ; (f) sat. 1 + sat. 2,  $\mathbf{v}_2$

position of the cluster of pixels of the binary maps. In the decentralized case, the corresponding isoranges are intersected to achieve the position estimate, whereas in the centralized case the target is directly localized. Fig. 3 shows the achieved results. As it can be observed, the decentralized strategy implies a significant dispersion of the position estimates. This is because the variation of the target signature among the bistatic channels and its extension over multiple resolution cells significantly increases the possibility to intersect isoranges corresponding to different positions, thus carrying to a solution that can be quite far from the actual ship location (represented by the black dotted lines). Particularly, it can be seen as the decentralized position estimates spread over the area highlighted by the isoranges passing for the bow and stern areas. In contrast, as in the proposed strategy the threshold is applied after multichannel data combination, the resulting position estimates are all concentrated around the area occupied by the target.

In the previous case study, we assumed that the local map corresponding to the actual target velocity has been selected. To verify the possibility to select the correct map under the challenging conditions of extended targets with varying signature over the different channels, the following case study is considered. Let us assume bow and stern be the dominant scatterers in the first and second bistatic channels, respectively, and the other scatterers showing a RCS 10 dBm<sup>2</sup> lower than the stronger point. For sake of clarity, a noise-free scenario is considered. The centralized approach is implemented for  $N = 10$  and  $T_f = 3$  s and for  $\mathbf{v}_1 = [3, 3]$  m/s (i.e., actual target

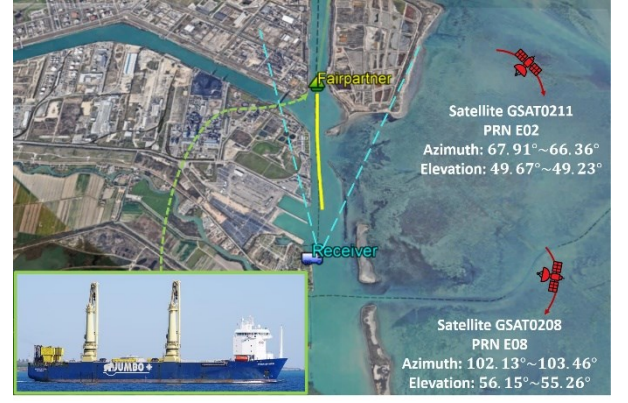


Fig. 5. Experimental acquisition geometry.

velocity) and  $\mathbf{v}_2 = [2.7, 2.5]$  m/s. Fig. 4 shows the resulting local maps, where 0 dB denotes the highest power observed among all the maps. Fig. 4 (a) and Fig. 4 (c) are the maps resulting from the multi-frame integration [i.e., summation over  $n$  only in (3)] corresponding to the actual target velocity for sat. 1 and sat. 2, respectively, where it can be seen as the target energy is well concentrated around the scatterers actual positions. In contrast, in the maps achieved by means of the inexact value of the target velocity, Fig. 4 (b) and (d), the multi-frame integration provided a lower integration gain, spreading the energy around larger areas, furthermore well outside the area occupied by the target. It can be observed as the scatterers ‘energies in the maps achieved for different tested velocities move along the bistatic isoranges. Consequently, the positions of the scatterers in the local maps pertaining the two bistatic geometries are the same when the actual target velocity is used, whereas otherwise differs. Therefore, despite the variation of the relative power levels in the different geometries, the same scattering centers overlap in the multistatic maps pertaining the actual target velocity [Fig. 4 (e)], while the resulting energy vanishes when other velocities are used [Fig. 4 (f)], resulting in a significantly lower IC. In the case study under consideration, IC with  $\mathbf{v}_1$  is equal to 16.76, while with  $\mathbf{v}_2$  is equal to 7.71. Therefore, by means of (4), the correct local map can be selected and the target correctly located.

#### IV EXPERIMENTAL RESULTS WITH GALILEO SATELLITES

Experimental acquisitions have been conducted at the Marghera port (Italy). Fig. 5 sketches the acquisition geometry. The receiver was observing the ships entering/exiting the terminal areas with a left hand circularly polarized antenna with gain 16 dBi and the Automatic Identification System (AIS) messages were also recorded to be used as ground truth. The cargo Fairpartner (143.1 m  $\times$  26.6 m, shown in the bottom box of Fig. 5) was moving away from the receiver, being in its field of view for 580 s. The signals transmitted by Galileo satellites GSAT0211 and GSAT0208 in the E5a band (hereafter, sat. 1 and sat. 2, respectively) were correctly tracked by the reference antenna and therefore used for the radar processing.

Fig. 6 shows the bistatic RD maps achieved with an integration window of 30 s (10 frames,  $T_f = 3$  s) after target motion compensation according to the AIS information, where the different target signature can be observed. Particularly, with

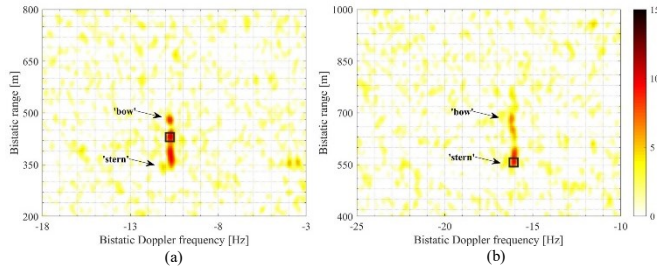


Fig. 6. Experimental multi-frame RD maps – (a) sat. 1; (b) sat. 2.

sat. 1, the ‘bow’ area of the target is more visible than with sat. 2, where the stronger returns are observed in the ‘stern’ area. The black ‘□’ markers denote the target centroid extracted from the maps by thresholding and clustering. It can be seen as the different behavior of the target response implied the selection of different target scattering centers.

Fig. 7 shows the integrated local map according to the velocity providing the highest IC (criteria for setting the velocity grid can be found in [7]). Thanks to the combination in square amplitudes implemented with the proposed strategy, all the different parts composing the target are well visible. By thresholding and clustering the resulting binary map, the centralized approach provides a position estimate quite close to the AIS position. In contrast, the extraction of target centroids corresponding to different scatterers in the bistatic maps brought the decentralized strategy to localize the target quite far from its actual location.

Finally, Fig. 8 shows the position estimates achieved over the target trajectory. The greater dispersion with the decentralized approach is quite evident, showing very large errors in few instants, while the centralized strategy provides estimates significantly closer to the AIS positions for the whole track. Taking the AIS as reference, the root-mean-square-error of the position estimate is 154.4 m for the decentralized approach, while it reduces to 64.0 m with the proposed strategy.

## V. CONCLUSION

This letter addressed the localization of ship targets with a passive radar system using multiple GNSS transmitters of opportunity and a single receiving station. A centralized strategy has been proposed to combine the data received over multiple bistatic channels and over multiple frames in a Cartesian reference system representing the surveyed area.

The presented analysis illustrated as the approach can bring significant improvements in target localization with respect to decentralized procedures, especially in the case of targets distributing over multiple resolution cells. These superior capabilities have been also confirmed by processing experimental data collected in a port area, thus verifying the effectiveness of the proposed strategy in real scenarios.

## ACKNOWLEDGMENT

The experimental campaigns were carried out inside the research project ‘GALILEO-BASED PASSIVE RADAR SYSTEM FOR MARITIME SURVEILLANCE - SpyGLASS’ funded from the European GNSS Agency under the European Union's Horizon 2020 research and innovation programme

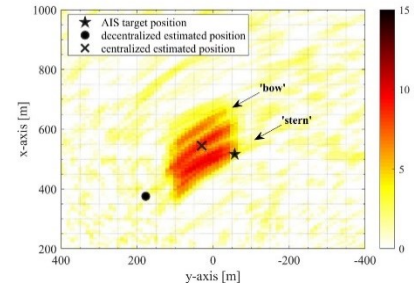


Fig. 7. Experimental integrated local map.

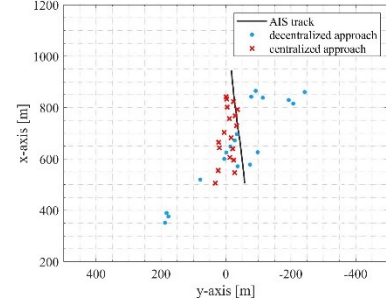


Fig. 8. Target track.

under grant agreement No. 641486.

## REFERENCES

- [1] H. Ma, M. Antoniou, D. Pastina, *et al.*, “Maritime moving target indication using passive GNSS-based bistatic radar,” *IEEE Trans. Aero. Elect. Syst.*, vol. 54, no. 11, pp. 115-130, Feb. 2018.
- [2] H. Ma, M. Antoniou, A.G. Stove, J. Winkel, M. Cherniakov, “Maritime moving target localization using passive GNSS-based multistatic radar,” *IEEE Trans. Geosci. Remote Sens.*, vol. 56, no. 8, pp. 4808-4819, Aug. 2018.
- [3] M. Sadeghi, F. Behnia, R. Amiri, “Maritime target localization from bistatic range measurements in space-based passive radar,” *IEEE Trans. Ins. Meas.*, vol. 70, pp. 1-8, Apr. 2021.
- [4] F. Santi, F. Pieralice, D. Pastina, “Joint detection and localization of vessels at sea with a GNSS-based multistatic radar,” *IEEE Trans. Geosci. Remote Sens.*, vol. 57, no. 8, pp. 5894-5913, Aug. 2019.
- [5] F. Santi, D. Pastina, M. Antoniou, M. Cherniakov, “GNSS-based multistatic passive radar imaging of ship targets,” *2020 IEEE Int. Radar Conf.*, pp. 601-606.
- [6] Z. Li, C. Huang, Z. Sun, *et al.*, “BeiDou-Based Passive Multistatic Radar Maritime Moving Target Detection Technique via Space-Time Hybrid Integration Processing,” *IEEE Trans. Geosci. Remote Sens.*, vol. 60, pp. 1-13, 2022.
- [7] D. Pastina, F. Santi, F. Pieralice, *et al.*, “Maritime moving target long time integration for passive GNSS-based bistatic radar,” *IEEE Trans. Aero. Elect. Syst.*, vol. 54, no. 11, pp. 115-130, Feb. 2018.
- [8] Q. Wu, Y. D. Zhang, M. G. Amin, B. Himed, “Space-time adaptive processing and motion parameter estimation in multistatic passive radar using sparse Bayesian learning,” *IEEE Trans. Geosci. Remote Sens.*, vol. 54, no. 2, pp. 944-957, Feb. 2016.
- [9] V.S. Chernyak, *Fundamentals of Multisite Radar Systems*, Gordon and Breach Science Publishers, CRC Press, 1998.
- [10] A.A. Gorji, R. Tharmarasa, T. Kirubarajan, “Widely separated MIMO versus multistatic radars for target localization and tracking,” *IEEE Trans. Aero. Elect. Syst.*, vol. 49, n. 4, pp.2179-2194, Oct. 2013.
- [11] B. Errasti-Alcala, W. Fuscaldo, P. Braca, G. Vivone, “Realistic ship model for extended target tracking algorithms,” *IEEE Int. Geosci. Remote Sens. Symp.*, 2015, pp. 3135-3138.
- [12] Z. He, Y. Yang, W. Chen, “A hybrid integration method for moving target detection with GNSS-based passive radar,” *IEEE J. Sel. Top. Appl. Remote Sens. Earth Obs.*, vol. 14, pp. 1184-1193, 2021.
- [13] X. Zhou, P. Wang, J. Chen, *et al.*, “A Modified Radon Fourier Transform for GNSS-Based Bistatic Radar Target Detection,” *IEEE Geosci. Remote Sens. Lett.*, vol. 19, pp. 1-5, 2022.